

Resonance Bonding Patterns of Peroxide Chemistry: Cyclic Three-Center Hyperbonding in “Phosphadioxirane” Intermediates

Jeremiah J. Wilke and Frank Weinhold*

Contribution from the Theoretical Chemistry Institute and Department of Chemistry,
University of Wisconsin, Madison, Wisconsin 53706

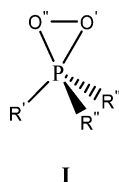
Received January 29, 2006; E-mail: weinhold@chem.wisc.edu

Abstract: We investigate the nature of valency and bonding in the highly unusual O_2PR_3 “phosphadioxirane” species recently isolated as an intermediate in the reaction of $^1\text{O}_2$ with organic phosphines PR_3 . Commonly, this species is depicted as a Lewis structure with five bonds at the phosphorus center, suggesting hypervalent involvement of extra-valence d-orbitals in the hybridization. However, nonhypervalent bonding patterns, such as open zwitterionic peroxides or $\text{R}_2\text{PO}_2^+\text{R}^-$ ion pairs, could also achieve the observed hypercoordination. In the present work, we employ *ab initio* and hybrid density functional calculations with theoretical analysis by means of Natural Resonance Theory (NRT) and Natural Bond Orbitals (NBOs) to investigate the role of valence shell expansion versus nonhypervalent ionic resonance in phosphadioxiranes. We find that true hypervalency is relatively negligible in phosphadioxiranes, and hypercoordination is instead achieved through both conventional linear Pimentel–Rundle three-center, four-electron (3c/4e) hyperbonding as well as an unprecedented *cyclic* form of 3c/4e hyperbonding. We examine ramifications and limits of the cyclic hyperbonding phenomenon in analogous carbon compounds and discuss some broader implications of its structural representation and nomenclature.

Introduction

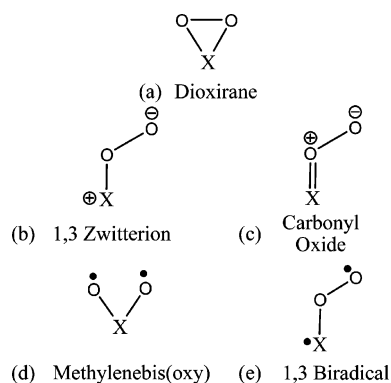
“Unusual peroxides”¹ have gained prominence both in theoretical² and experimental studies^{3–6} as either putative intermediates or isolated species in oxidation reactions. The set of species having the general molecular formula XO_2 ($\text{X} = \text{CH}_2, \text{SH}_2, \text{PH}_3$) represents a special class of oxidizing agents which can operate by nonradical mechanisms. Several logical Lewis structures are possible for these species, as shown in Chart 1. Each localized bond pattern may be the dominant representation of a unique equilibrium structure or a single resonance contribution to a resonance hybrid. In general, the contribution of a given resonance structure to a composite resonance hybrid should be reflected in species structure and reactivity. For example, increased carbonyl oxide character in a given species may be expected to promote reactivity patterns associated with the parent carbonyl oxide, such as [3 + 2]-cycloaddition in Criegee-type reactions or nucleophilic O-atom transfer in the oxidation of sulfoxides.

Phosphine peroxides having the nominal Lewis structure representation⁷ **I** have gained importance in the reactions of



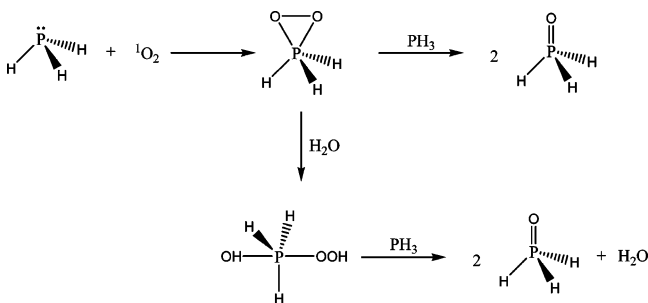
phosphines and phosphites with singlet oxygen (Scheme 1). The first experimental isolation of a “phosphadioxirane” was recently

Chart 1. Possible Structures for Peroxidic Intermediates (with names for $\text{X} = \text{CH}_2$)



reported by Selke et al.⁴ from the reaction of tris(*o*-methoxyphenyl)phosphine with $^1\text{O}_2$. Some aspects of the geometry and energetics of phosphadioxirane reactions were also characterized theoretically by Nahm et al.² for compounds with $\text{R}' = \text{R}'' = \text{H}$ and CH_3 . The dioxirane-like ring geometry was found to be a ubiquitous feature of these species, rather independent of method and basis set.

- (1) Greer, A. *Science* **2003**, *302*, 235–236.
- (2) Nahm, K.; Li, Y.; Evanseck, J. D.; Houk, K. N.; Foote, C. S. *J. Am. Chem. Soc.* **1993**, *115*, 4879–4884.
- (3) Gao, R.; Ho, D. G.; Dong, T.; Khuu, D.; Franco, N.; Sezer, O.; Selke, M. *Org. Lett.* **2001**, *3*, 3719–3722.
- (4) Ho, D. G.; Gao, R.; Celaje, J.; Chung, H.; Selke, M. *Science* **2003**, *302*, 259–262.
- (5) Tsuji, S.; Kondo, M.; Ishiguro, K.; Sawaki, Y. *J. Org. Chem.* **1993**, *58*, 5055–5059.
- (6) Nakamoto, M.; Akiba, K. *J. Am. Chem. Soc.* **1999**, *121*, 6958–6959.

Scheme 1. Reaction of Phosphine and Singlet Oxygen to Yield Phosphine Oxide

Experimentally, phosphadioxiranes are expected to exhibit spectral similarities to high oxidation state transition metal complexes with dioxygen,⁸ to epoxidize olefins,⁴ and to yield an electrophilic Hammett profile when reacting with aryl sulfides.⁵ Phosphadioxiranes therefore seem best classified as an oxene-like electrophilic oxidant, most consistent with resonance formulation **I**. In this respect, phosphine peroxides appear distinct from sulfur^{9–13} and carbon¹⁴ peroxides, which have distinct isomeric cyclic and open geometries corresponding to electrophilic and nucleophilic forms, respectively.

Despite the recent focus on unusual peroxides^{1,9,13,14} and other hypervalent ring compounds,¹⁵ to our knowledge, no attempt has been made to characterize phosphadioxiranes in more precise electronic terms using analysis of charge densities, bond orders, or other aspects of the formal hybridization and bonding pattern. A qualitative picture of bonding in phosphadioxirane-type peroxides presents a fundamental valency problem. In enium peroxides, such as dioxirane (O₂CH₂) and dioxaziridine (O₂NH), the central atom must only accommodate four electron pairs (e.g., four bonds in dioxirane or three bonds and one lone pair in dioxaziridine). The cyclic structure (Chart 1a) is therefore octet-conforming, requiring only valence shell hybrids. Furthermore, ring opening leaves an unoccupied p-orbital on the central atom, and cyclization is therefore strongly favored over 1,3-zwitterionic structures (Chart 1b). However, in the case of onium peroxides, such as X = PH₃, cyclization from the 1,3-zwitterionic structure must violate standard covalency rules since there are no valence shell p-orbitals to accept the incoming lone pair and form a two-center bond. The hypercoordination at phosphorus as well as the electrophilic reactivity initially suggests that phosphadioxirane should be represented by hypervalent Lewis representation **I**. However, structure **I** implies expansion of the sp valence shell to include d-orbitals in the skeletal hybridization (e.g., sp³d hybrids of 20% d-character). While d-based hybridization was frequently postulated in the past, ab initio evidence has tended to discount the role of d-orbital participation in main-group hypervalency.^{16–20}

(7) Throughout the work, we employ the labeling scheme shown in **I**, where R' refers to the phosphine substituent coplanar with the phosphorus–oxygen ring (pseudoapical) and R'' refers to the two out-of-plane substituents (pseudoequatorial) (cf. resonance structure **I**). Furthermore, we refer to the oxygen nearer the R' substituent as O' (pseudoequatorial) and the oxygen nearer the R'' substituents as O'' (pseudoapical).

(8) Reynolds, M. S.; Butler, A. J. *Inorg. Chem.* **1996**, *35*, 2378–2383.

(9) Sawaki, K.; Ishiguro, K. *Bull. Chem. Soc. Jpn.* **2000**, *73*, 535–552.

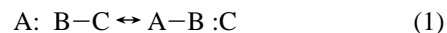
(10) Jensen, F.; Greer, A.; Clennan, E. L. *J. Am. Chem. Soc.* **1998**, *120*, 4439–4449.

(11) Sawaki, Y.; Watanabe, Y.; Kuriki, N.; Ishiguro, K. *J. Am. Chem. Soc.* **1991**, *113*, 2677–2682.

(12) Foote, C. S.; Liank, J.; Gu, C. L.; Kacher, M. L. *J. Am. Chem. Soc.* **1983**, *105*, 4717–4721.

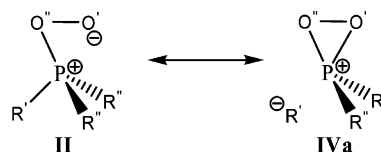
(13) McKee, M. L. *J. Am. Chem. Soc.* **1998**, *120*, 3963–3969.

In contrast to formal hypervalency, the three-center MO theory of Pimentel²¹ and Rundle^{22,23} suggests how hypercoordination can readily be achieved *within* the framework of ordinary valence sp-hybridization. As pointed out by Coulson,²⁴ the Pimentel–Rundle three-center (3c), four-electron (4e) model of hypervalent A···B···C bonding is equivalent to the contribution of two strong resonance structures of the form



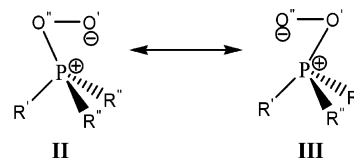
Octet-violating hypervalency at the central atom B is averted because the A···B and B···C linkages each correspond to approximate half-bonds (formal bond orders $b_{AB} \cong b_{BC} \cong 0.5$). It has been suggested that the characteristic 3c/4e bonding motif be denoted by a special symbol (ω_{ABC}) and nomenclature (ω -bonding or hyperbonding) to indicate its distinctive electronic features.²⁵ In the language of formal charges [viz., A:–B⁺–C ↔ A–B⁺:C[–] for the resonance structures in eq 1], the Pimentel–Rundle picture also corresponds to the inclusion of partial ionic character to avert hypervalency.

The Pimentel–Rundle three-center MO picture can be succinctly described in the language of Natural Bond Orbital (NBO) theory.^{26–28} In NBO language, ω_{ABC} -bonding is represented by strong donor–acceptor interactions of type $n_A \rightarrow \sigma^*_{BC}$ (delocalization from the valence lone pair orbital n_A of A: into the valence antibonding orbital σ^*_{BC} of B–C in the $\text{A}^- \text{B}^+ \text{C}$ structure, or equivalently, of type $n_C \rightarrow \sigma^*_{AB}$ in the $\text{A–B}^+ \text{:C}^-$ structure). In the case of phosphadioxirane, the most obvious ω -bonding corresponds to a conventional linear hyperbond occurring in the resonance between zwitterionic structure **II** and ion-pair structure **IVa**. The phosphorus center therefore acquires

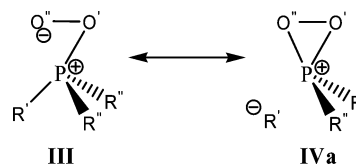


strong cationic character, while the pseudo-apical oxygen and phosphine substituent acquire anionic character.

Another possible resonance could occur between zwitterionic structures **II** and **III** or between zwitterionic structure **III** and



ion-pair structure **IVa**. Corresponding $\omega_{O'PR''}$ (**IVb**, **IVc**) struc-



tures could also occur for out-of-plane substituents. As will be

(14) Murray, R. W. *Chem. Rev.* **1989**, *89*, 1187–1201.

(15) Inagaki, S.; Ikeda, H. *J. Phys. Chem. A* **2001**, *105*, 10711–10718.

(16) Kutzelnigg, W. *Angew. Chem., Int. Ed. Engl.* **1984**, *23*, 272–295.

(17) Magnusson, E. *J. Am. Chem. Soc.* **1990**, *112*, 7940–7951.

(18) Reed, A. E.; Schleyer, P. v. R. *J. Am. Chem. Soc.* **1990**, *112*, 1434–1445.

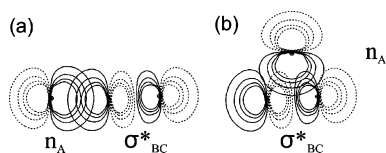
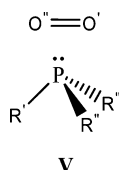


Figure 1. (a) Most favorable geometry for $n_A \rightarrow \sigma^*_{BC}$ interaction (overlap of lone pair with backside lobe of antibond). (b) Unfavorable geometry for $n_A \rightarrow \sigma^*_{BC}$ interaction (overlap of lone pair with middle node).

shown in the Results, hyperbonds corresponding to each of these resonance motifs contribute appreciably to the phosphadioxirane electronic structure.

An alternative nonhypervalent resonance picture may be represented as a π -complex (**V**) that involves no formal P–O bonding



Because resonance structures **I–V** (and others that could be imagined) suggest quite different pictures of the charge distribution, bond strengths, hybridization, and reactivity pattern, the actual resonance hybrid may represent a complex mixture of some or all of these limiting, idealized depictions.

Given the alternative pictures of hypervalency in phosphorus compounds,^{15,16,18,29} it remains unclear whether phosphadioxirane is best described by a 3c/4e model, d-orbital hypervalency, or some other formulation. Previous literature has often favored 3c/4e bonding or other octet-conforming formulations in describing apparently hypervalent species.^{16–18} However, phosphadioxirane is distorted from the idealized trigonal bipyramid, straining the linear arrangements that are commonly considered necessary for a 3c/4e interaction. To maximize $n_A \rightarrow \sigma^*_{BC}$ donor–acceptor overlap, one might consider that the most likely exposure of the σ^*_{BC} orbital to the incoming nucleophile is the backside lobe of the antibond (Figure 1a), favoring near-linear geometry.²⁵ Resonance between cyclic, zwitterionic structures **II** and **III** or between **III** and **IVa**, in contrast, would seem to force the donor lone pair to encounter a nodal plane in the antibond in the enforced nonlinear geometry (Figure 1b). Despite the close proximity of the oxygen lone pairs and P–O antibonds in a cyclic geometry, a 3c/4e interaction therefore does not seem likely within the PO₂ heterocycle. Phosphadioxiranes therefore raise some classic bonding questions in a new and perplexing way.

In the present work, we extend the studies of Nahm et al.² and Inagaki¹⁵ by using ab initio and density functional calculations to establish a quantitative resonance-type description of

the valency and bonding in the parent species O₂PH₃. We employ the NBO-based Natural Resonance Theory (NRT)^{30–32} to determine the relative resonance contributions of structures **I–V**. We also consider the structural and electronic dependence of phosphadioxirane on the inclusion or noninclusion of d-type basis functions. Specifically, we examine whether hypercoordination at the phosphorus center is achieved through valence shell expansion to d-orbitals or through valence shell resonance involving 3c/4e hyperbonding or another octet-compliant motif. We also attempt to put the phosphorus species into the broader perspective of enium and onium peroxides and the more general transformations that result from dioxygen additions at main-group centers.

Theoretical Analysis Methods and Computational Model

Natural Resonance Theory. Briefly and somewhat heuristically, the NRT algorithm^{30–32} determines a normalized set of non-negative resonance weightings, $\mathbf{w} = \{w_1, w_2, \dots\}$, that optimally represent the total electron density (ρ_{full}) as a weighted, convex combination of idealized densities (ρ_r) of individual resonance structures, r .

$$\rho_{\text{full}} = \sum_r^{RS} w_r \rho_r \quad (w_r \geq 0, \sum_r^{RS} w_r = 1) \quad (2)$$

The accuracy of the NRT description is quantified by the root-mean-square deviation, $d(\mathbf{w})$, of the idealized resonance superposition from the true density, which is minimized by the NRT variational algorithm.

$$d(\mathbf{w}) = \min_{\mathbf{w}} \left\{ \frac{1}{n} \sum_{i=1}^n (\bar{q}_i - q_i)^2 \right\}^{1/2} \quad (3)$$

Here, \bar{q}_i is the variationally selected, resonance-weighted occupancy of the i th NBO, and q_i is the exact NBO occupancy in the full molecular wavefunction. Equivalently, the NRT “fit”, $f(\mathbf{w})$, is quantified by the fractional improvement ($0 \leq f \leq 1$) with respect to the best *single-term* description, $d(0)$, which is maximized in the NRT variational optimization.

$$f(\mathbf{w}) = 1 - \frac{d(\mathbf{w})}{d(0)} \quad (4)$$

The NRT algorithm is based on the primary role of a leading set of “reference” Lewis structures. By default, NRT analysis attempts to identify these strongly weighted reference structures whose *full* density matrices enter the variational minimization (eq 3), as opposed to the lesser-weighted secondary structures whose weightings are computed by a simpler perturbative estimate. To ensure that a given set of resonance structures is treated in a uniform manner, a group of reference structures can be explicitly specified using the \$NRTSTR keylist, forcing a balanced comparison of their resonance weightings even if one or more did not achieve reference status in the default NRT search. This strategy is employed in the present work to ensure that the weightings of structures **I–V** are considered in a balanced manner for all species to be considered, even when the weightings of some of these structures are negligibly small in one species or another. For a given set of multi-reference resonance weightings, \mathbf{W} , values of $D(\mathbf{W})$ and $F(\mathbf{W})$ [analogous to $d(\mathbf{w})$ and $f(\mathbf{w})$ in (eqs 3 and 4)] are then obtained that quantify the RMS deviation and fractional improvement of the multi-reference treatment over the single reference treatment. In default

- (19) Musher, J. I. *Angew. Chem.* **1969**, *8*, 54–68.
 (20) Musher, J. I. *J. Am. Chem. Soc.* **1972**, *94*, 1370–1371.
 (21) Pimentel, G. C. *J. Chem. Phys.* **1951**, *19*, 446–448.
 (22) Rundle, R. E. *J. Am. Chem. Soc.* **1947**, *69*, 1327–1331.
 (23) Rundle, R. E. *J. Chem. Phys.* **1949**, *17*, 671–675.
 (24) Coulson, C. A. *J. Chem. Soc.* **1964**, 1442–1454.
 (25) Weinhold, F.; Landis, C. R. *Valency and Bonding: A Natural Bond Orbital Donor–Acceptor Perspective*; Cambridge University Press: Cambridge, U.K., 2005; pp 275–306.
 (26) Foster, J. P.; Weinhold, F. *J. Am. Chem. Soc.* **1980**, *102*, 7211–7218.
 (27) Reed, A. E.; Weinhold, F. *J. Chem. Phys.* **1983**, *78*, 4066–4073.
 (28) Reed, A. E.; Weinstock, R. B.; Weinhold, F. *J. Chem. Phys.* **1985**, *83*, 735–746.
 (29) Molina, J. M.; Dobado, J. *Theor. Chem. Acc.* **2001**, *105*, 328–337.

- (30) Glendening, E. D.; Weinhold, F. *J. Comput. Chem.* **1998**, *19*, 593–609.
 (31) Glendening, E. D.; Weinhold, F. *J. Comput. Chem.* **1998**, *19*, 610–627.
 (32) Glendening, E. D.; Badenhop, J. K.; Weinhold, F. *J. Comput. Chem.* **1998**, *19*, 628–646.

mode, the NRT search considers valence shell resonance structures only, but for the sake of balance in the present case, the NRTFDM keyword (full density matrix space) is employed to ensure that all possible d-shell and other nonvalence shell contributions are allowed from any structure. The original papers^{30–32} and NBO 5.0 program documentation³³ should be consulted for a more detailed description of the NRT variational algorithm and its numerical implementation in the current NBO 5.0 program.

NBOs and Non-Lewis Occupancy of Selected (\$CHOOSE Key-list) Resonance Structures. By default, the NBO analysis determines the best possible single Lewis structural description of the wavefunction. Remaining delocalization corrections are represented as donor–acceptor interactions between occupied and unoccupied orbitals of the Lewis-like picture. The former are referred to as Lewis orbitals, consisting of one-center core orbitals, lone pairs (n_A), and two-center bonding orbitals (σ_{AB} , π_{AB}). The latter are referred to as non-Lewis orbitals, consisting of two-center valence shell antibonding orbitals (σ_{AB}^* , π_{AB}^*) and one-center extra-valence Rydberg orbitals (ry_A^*).^{27,28} The total non-Lewis occupancy (ρ_{NL}) measures the residual “error” of the indicated Lewis-like description. Remaining delocalization corrections are usually well accounted for by low-order perturbative estimates. Specifically, the strength of a given delocalization from an occupied donor orbital, φ_i , to an unoccupied acceptor orbital, φ_{j^*} , can be estimated using the second-order perturbative correction.^{34,35}

$$\Delta E_{i \rightarrow j^*} = -n_i \frac{F_{ij}^2}{\epsilon_{j^*} - \epsilon_i} \quad (5)$$

Here n_i is the occupancy of the donor orbital and $F_{ij} = \langle \varphi_i | \hat{F} | \varphi_{j^*} \rangle$ is the Fock (Kohn–Sham) matrix element between φ_i and φ_{j^*} . Because F_{ij} is often approximately proportional to the overlap between the orbitals,³⁶ graphical overlap plots give a useful visual estimate of the interaction strength. Contour and 3-D surface plots of the NBOs, obtainable with the NBOView 1.0 program,³⁷ therefore effectively complement the perturbative estimates of NBO interactions. Note that the NBO description does not alter any quantitative features of the potential energy surface, but is merely a more informative way to describe the original DFT calculations from which the NBOs are derived.

In a situation where a single Lewis structure is inadequate, the \$CHOOSE keylist can be employed to override the default NBO search in favor of a selected alternate bonding pattern. The \$CHOOSE search again optimizes the details of the NBOs (i.e., hybridization, polarization coefficients) for the chosen \$CHOOSE structure, with resultant non-Lewis occupancy, ρ_{NL} , that quantifies the error of the structure. The \$CHOOSE search with associated ρ_{NL} value thereby provides a complementary alternative to NRT for estimating the relative accuracy of any chosen resonance structure and for preselecting the leading reference structures to be included in full NRT treatment.

(33) Glendening, E. D.; Badenhoop, J. K.; Reed, A. E.; Carpenter, J. E.; Bohmann, J. A.; Morales, C. M.; Weinhold, F. *NBO 5.0*; Theoretical Chemistry Institute, University of Wisconsin, Madison, WI, 2001; F. Weinhold, F., Ed. *NBO 5.0 Program Manual*; Theoretical Chemistry Institute, University Wisconsin, Madison, WI, 2001.

(34) Reed, A. E.; Curtiss, L. A.; Weinhold, F. *Chem. Rev.* **1988**, *88*, 899–926.

(35) Weinhold, F. Natural Bond Orbital Methods. In *Encyclopedia of Computational Chemistry*; Schleyer, P. v. R., Allinger, N. L., Clark, T., Gasteiger, J., Kollman, P. A., Schaefer, H. F., Schreiner, P. R., Eds.; John Wiley and Sons: Chichester, U.K., 1998; Vol. 3, pp 1792–1811.

(36) For visualization purposes, orbital diagrams display the pre-orthogonal PNBO associated with each NBO. While NBOs are constructed from natural atomic orbitals (NAOs) having the property of interatomic orthogonality, corresponding PNBOs, $\hat{\varphi}_i$, are constructed from pre-orthogonal NAOs (PNAOs). The PNBO retains the same hybridization and polarization coefficients as the parent NBO preserving the essential nature of the orbital interaction while maintaining an intuitive picture of the overlap. The PNBO overlap diagrams therefore effectively complement the numerical estimates (eq 5), calculated from NBOs.

(37) All contour and surface plots were performed with the *NBOView 1.1: NBO Orbital Graphics Program*; Wendt, M.; Weinhold, F., 2001, Board of Regents of the University of Wisconsin System; Weinhold, F. *NBOView: NBO Orbital Graphics Plotter*; http://www.chem.wisc.edu/~nbo5/v_manual.htm (accessed 10/13/2004).

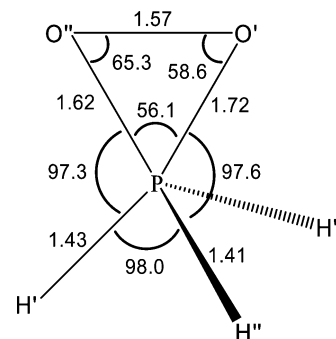


Figure 2. Bond lengths (Å) and bond angles (deg) for O_2PH_3 at the B3LYP/6-31+G* level.

Optimizations and Single-Point Calculations. All species described in the present work were calculated at the B3LYP/6-31+G*/B3LYP/6-31+G* level using the Gaussian 98 package.^{38,39} All B3LYP-calculated species were checked for possible stationary-point instability (by verifying that the vibrational frequencies are all positive) and for biradical or other electronic instability (by using the STABLE=OPT keyword). Numerous geometry optimizations were carried out on phosphodioxirane with other methods (HF, MP2, QCISD(T)) and basis sets (3-21G, aug-cc-pVDZ, aug-cc-pVTZ), while NRT and NBO analyses were also carried out on the MP2 and HF wavefunctions to establish that the presented results are robustly representative.⁴⁰

Results and Discussion

Geometry. We investigated a large variety of O_2PR_3 species ($R = F, CN, CH_3, C_2H_5$), but for simplicity, only the results for $R' = R'' = H$ are discussed in detail here. Selected results for other substituents demonstrate the generality of the results across varying electronegativity and π -donor/acceptor character, as summarized in the Supporting Information. In agreement with the results of Nahm et al.,² we were unable to locate any open peroxidic or zwitterionic structures on the O_2PH_3 potential energy surface. All calculated phosphodioxirane equilibrium structures were found to be C_s -symmetric, with the plane of symmetry containing the PO_2 ring and one of the substituents (Figure 2). The species can be considered to have a pseudoapical hydrogen, H' , and oxygen, O' , as well as pseudoequatorial hydrogens, H'' , and oxygen, O'' , as labeled in the figure.

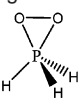
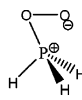
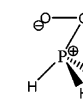
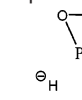
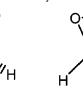
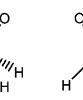
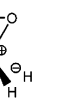
Natural Resonance Theory Analysis. On the basis of preliminary \$CHOOSE and NRT analyses for a variety of substituents and geometries, four leading resonance structures were selected for inclusion in the initial NRT reference set (**I**, **II**, **III**, and the π -complex **V**). These structures and the associated resonance weightings are detailed pictorially in Table 1. The highest weighting for a single structure in this four-reference treatment is that of **II**, 32.7%. No single Lewis structure is therefore adequate to describe the total electron density. In the four-reference calculation, the weighting of the hypervalent structure **I** is 18.1% (Table 1), comparable to the weightings of **II** (32.7%) and **III** (20.7%). The formal covalency

(38) Foresman, J. B.; Frisch, A. *Exploring Chemistry With Electronic Structure Methods: A Guide to Using Gaussian*, 2nd ed.; Gaussian Inc.: Pittsburgh, PA, 1996.

(39) Frisch, M. J.; et al. *Gaussian 98*, revision A.9; Gaussian Inc.: Pittsburgh, PA, 1998.

(40) It may be noted in passing that weak UHF-type instabilities were found in some lower level HF calculations, whereas B3LYP calculations and HF calculation with a larger basis set (e.g., aug-cc-pVTZ) were generally free of such instabilities. The general tendency for greater robustness of DFT solutions to biradical-like instability in comparison to HF solutions has been previously noted: (a) Ahlrichs, R.; Bauernschmitt, R. *J. Chem. Phys.* **1996**, *104*, 9047–9052. (b) Cremer, D. *Mol. Phys.* **2001**, *99*, 1899–1940.

Table 1. NRT Resonance Weightings for Peroxidic Structures for Phosphadioxirane, as Calculated with Different Reference Sets (see text)

							
	I	II	III	IVa	IVb	IVc	V
4-Ref^a	18.1	32.7	20.7	2.9	<1.0	<1.0	6.1
7-Ref^b	4.8	30.5	19.3	10.3	4.6	4.5	5.0
6-Ref^c	<1.0	32.2	20.5	11.0	5.0	4.8	6.1

^a Reference: **I, II, III**, and **V**. ^b Reference: all structures **I–V**. ^c Reference: **II–V**.

Table 2. RMS Deviation [$D(W)$, eq 3] and Fractional Improvement [$F(W)$, eq 4] for Multi-Reference Treatments of O_2PH_3

reference set	4-Ref ^a	7-Ref ^b	6-Ref ^c	6-Alt ^d
$D(W)$	0.0187	0.0179	0.0179	0.0194
$F(W)$	0.187	0.222	0.221	0.185

^a Reference: **I, II, III**, and **V**. ^b Reference: all structures **I–V**. ^c Reference: **I–IVc**. ^d Similar to 6-Ref treatment, with **II** removed and **I** added.

of the phosphorus center was calculated to be 3.08, suggesting only modest expansion of the valence shell with d-orbitals beyond nominal phosphorus trivalency.

In the four-reference calculation, the ion-pair structure **IVa** had a small but significant weighting (2.9%), suggesting it may warrant inclusion in the reference set. A second calculation was therefore carried out to examine the relative weightings of the ion-pair structures **IVa–IVc** against structure **I**. Seven structures were thereafter included in the expanded reference set (**I–III**, **IVa–IVc**, and **V**). The combined weighting of **IVa–IVc** in the seven-reference treatment is approximately 16% higher than their weighting in the four-reference treatment. Concurrently, the weighting for **I** is significantly diminished to less than 5%. The seven-reference calculation therefore suggests that, when **IVa–IVc** are included along with the hypervalent formulation **I** as reference structures, the closed ring character of phosphadioxirane **I** is better described as an admixture of the ion-pair structures.

Two final NRT calculations were performed to evaluate whether structure **I** is even required in the reference set for phosphadioxirane. A calculation with six resonance structures was performed by removing **I** from the seven-reference set (Table 1). The weighting of **I** decreases to a negligible amount ($\ll 1\%$) when removed from the reference set. Meanwhile, the RMS deviation, $D(W)$, and fractional improvement, $F(W)$ (vide supra), values remain effectively constant (Table 2), demonstrating that inclusion of **I** in the reference set adds no appreciable accuracy to the resonance description. In contrast, an analogous calculation with **II** removed and **I** added (6-Alt) results in decreases in both the $D(W)$ and $F(W)$ values (Table 2), demonstrating the greater importance of the zwitterionic structures. The NRT results therefore suggest that the most common hypervalent Lewis structure **I** contributes only minimally to the resonance description of the total wavefunction, consistent with the rather negligible d-occupancy and near trivalency of phosphorus.

NBO Analysis and \$CHOOSE Structures. Although the low weighting of **I** in the seven-reference NRT treatment suggests that it is a poor description of the phosphadioxirane electronic structure, the non-Lewis occupancy of **I** is only 0.64e or 1.9% of the total electron density, lower than the non-Lewis

Table 3. Phosphorus-Based σ -Bond NBOs and Occupancies (total and phosphorus d_p -type) for \$CHOOSE Structure **I**, Showing Polarization Coefficient (c_p) and Hybrid (h_p) (with percent s/p/d character) for Each $\sigma_{PX} = c_p h_p + c_x h_x$

NBO	Occupancy			h_p	% s	% p	% d
	total (e)	d_p (e)	c_p				
PH'	1.80	0.23	0.64	sp ^{2.1} d ^{1.4}	23	47	31
PH''	1.93	0.09	0.70	sp ^{2.9} d ^{0.4}	23	67	9
PO'	1.92	0.09	0.39	sp ^{4.3} d ^{2.5}	13	55	32
PO''	1.94	0.08	0.44	sp ^{3.4} d ^{1.1}	18	62	20

occupancies of the other reference structures. However, the Natural Atomic Orbital (NAO)⁴¹ estimate of the total d-occupancy of phosphorus is only 0.09e, inconsistent with the significant d-occupancy expected from structure **I**. Using the \$CHOOSE keylist forces the NBO routine to fit a set of two-center bonds to structure **I**, resulting in apparent d-occupancies of the phosphorus NBOs which are significantly higher than the actual NAO occupancies (Table 3). Despite its apparent performance as the best *single* structure match to the total wavefunction, **I** alone is therefore a misleading description of the electronic structure. We restrict subsequent \$CHOOSE discussion to structures **II–IVc**.

Leading Donor–Acceptor Interactions. In structures **II** and **III**, the anionic oxygen has three lone pairs: the first is an s-rich hybrid in the plane of the ring and pointing outward, the second is a p-rich hybrid perpendicular to the plane of the ring, and the third is an sp hybrid pointing into the plane of the ring. In structure **II**, the unoccupied P–H' antibond intuitively presents itself for favorable overlap with the third oxygen lone pair, given the approximately linear arrangement. A large vicinal delocalization is therefore observed in both the overlap plot (Figure 3) and the perturbative estimate of the interaction strength, 39.6 kcal/mol. Conversely, the backside lobe of the P–O' antibond overlaps strongly with the hydride lone pair in ionic structure **IVa**, with an associated interaction strength of 126.2 kcal/mol (Figure 4). This reciprocal $n_{H'} \rightarrow \sigma^*_{PO'} : n_{O'} \rightarrow \sigma^*_{PH'}$ delocalization pattern suggests the existence of significant linear ω -bonding.

The framework of structures **II** and **III** is more complicated. Given the strained geometry of the PO₂ ring ($\angle O'–P–O'' = 56.1^\circ$), no regions of the P–O antibond intuitively present themselves for overlap with an opposing oxide lone pair. The s-rich and p-rich hybrids point away from the P–O antibond

(41) Natural atomic orbitals are formed from the orthogonalization of atomic orbitals between all atoms in the molecule. This preserves the essential one-center character of the orbitals, but yields the necessary interatomic orthogonality. The NAO estimate of the d-occupancy results from adding up the d-occupancy in all of the phosphorus atomic orbitals and, in that sense, is more fundamental than the NBO picture, which carries the intrinsic non-Lewis “error” of the assignment.

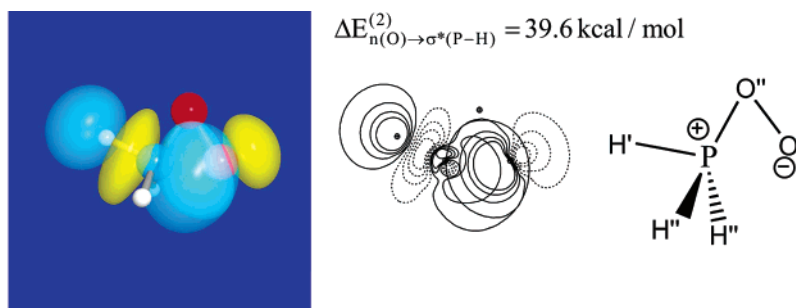


Figure 3. Three-dimensional surface view (left), contour plot (middle), and resonance structure (right) for the $n(O') \rightarrow \sigma^*(PH')$ interaction. Standard NBO settings are employed with outer contour (surface) at 0.0316 with 0.05 intervals for the four outermost lines in the contour plot.

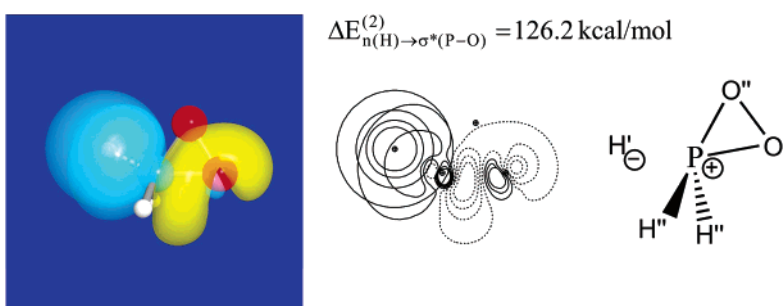


Figure 4. Similar to Figure 3, for the $n(H') \rightarrow \sigma^*(PO')$ interaction.

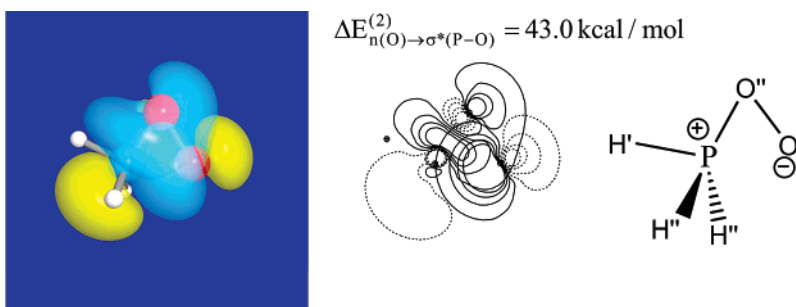


Figure 5. Similar to Figure 3, for the $n(O'') \rightarrow \sigma^*(PO'')$ interaction.

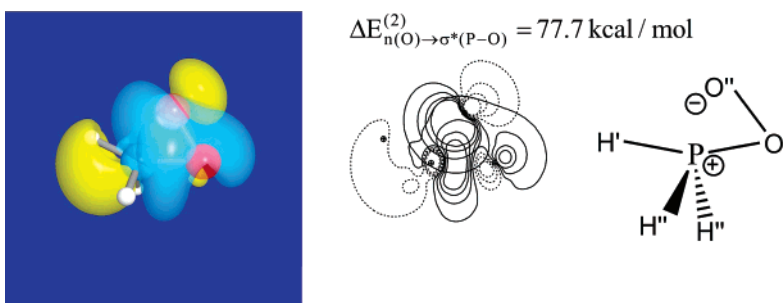


Figure 6. Similar to Figure 3, for the $n(O''') \rightarrow \sigma^*(PO''')$ interaction.

and, therefore, do not overlap significantly. Furthermore, the sp lone pair is expected to encounter a nodal plane in the $P-O$ antibond, resulting in low net overlap and weak interaction. Surprisingly, however, the oxygen–phosphorus ring still exhibits the robust reciprocal $n_{O'} \rightarrow \sigma^*_{PO''}$ and $n_{O''} \rightarrow \sigma^*_{PO'}$ interactions characteristic of three-center bonds. The strength of the interaction between the O' sp lone pair and the $P-O''$ antibond in **II** is found to be 43.0 kcal/mol, and an analogous $n_{O''} \rightarrow \sigma^*_{PO'}$ interaction in **III** is 77.7 kcal/mol, indicative of highly significant stabilizations.

Orbital plots suggest an explanation for the surprisingly large delocalizations. The plots (Figures 5 and 6) clearly reveal that

the polarity of the $P-O$ bond places the *middle* lobe of the antibond in a fortuitous position for interaction with the oxide lone pair. The unique form of the bonding hybrids in O_2PH_3 therefore leads to a novel form of *cyclic* three-center character, to our knowledge not previously recognized.

Similar interactions $n_{O''} \rightarrow \sigma^*_{PH'}$ and $n_{H'} \rightarrow \sigma^*_{PO''}$ occur in structures **III** and **IVa**, respectively. Analogous to $\omega_{O'PO''}$, such delocalizations do not initially seem feasible, given the strained geometry ($\angle O''-P-H' = 97.3^\circ$). The novel form of inner-lobe three-center bonding, however, resolves the difficulty again through the position of the antibonds and lone pairs (Figures 7 and 8) which engage in strong complementary $n_{O'} \rightarrow \sigma^*_{PH'}$ and

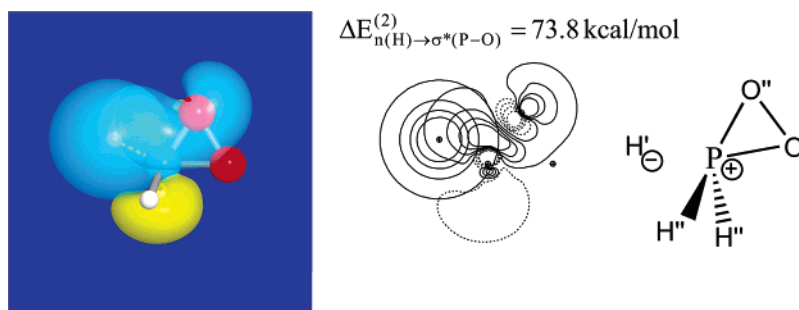


Figure 7. Similar to Figure 3, for the $n(H') \rightarrow \sigma^*(PO'')$ interaction.

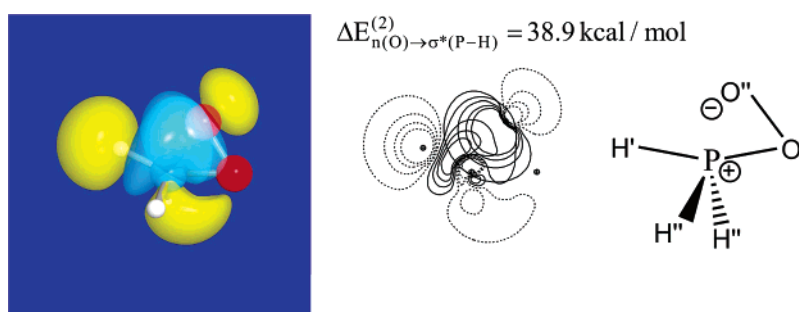


Figure 8. Similar to Figure 3, for the $n(O'') \rightarrow \sigma^*(PH')$ interaction.

$n_{H'} \rightarrow \sigma^*_{PO''}$ interactions. The cyclic hyperbonding phenomenon therefore overcomes the superficially unfavorable geometrical constraints, allowing O_2PH_3 to achieve a pentacoordinated structure through an unusual form of valence shell resonance.

The hyperbonding motif accounts for the observation that only cyclic equilibrium geometries could be located for O_2PH_3 . Nahm et al. hypothesized that only the cyclic species exists since the oxide lone pair of O' in **II** must always be anti to a P–H antibond.² The present results are consistent with this hypothesis. Forming a more open, zwitterionic species must sacrifice delocalizations of the oxygen lone pair $n_{O'} \rightarrow \sigma^*_{PH'}$ and $n_{O'} \rightarrow ry^*_P$ into the P–H' antibond and phosphorus $3d_{xz}$ -orbital, respectively. Furthermore, the hyperbonds $\omega_{O'PO''}$ and $\omega_{O''PH'}$ contribute extra stability to the ring geometry, reducing the energetic cost of the highly strained bonds.

We also comment briefly on the expected robustness of the $3c/4e$ motif with respect to variations in substituent electronegativity or steric bulk (as documented in the Supporting Information for $R = F, CN, CH_3, C_2H_5$ substituents). In accordance with Bent's rule,⁴² more electronegative substituents are expected to have three main effects:

(i) The phosphorus hybrids acquire increased p-character in the P–R bonds and increased s-character in the P–O bonds, with the latter change tending to shorten the P–O bonds and open the O–P–O angle.

(ii) The greater P–R polarity increases the resonance weighting of ion-pair structures, resulting in reduced P–R bond order but increased P–O bond order, which again favors shorter P–O distance.

(iii) A more electronegative R substituent increases the amplitude of the P–R antibond at the phosphorus center, thereby strengthening the $n_{O'} \rightarrow \sigma^*_{PR'}$ and $n_{O''} \rightarrow \sigma^*_{PR''}$ interactions and tending to linearize the O–P–R linkages.

The electronegativity trends can all be seen for the cases of $R = F, CN,$ or CH_3 as described in the Supporting Information.

Table 4. Bond Lengths A–B (Å) and Angles A–B–C (deg) in O_2PH_3 , with (6-31+G*) and without (6-31+G) d-Functions

	6-31+G*	6-31+G
P–H'	1.43	1.46
P–H''	1.41	1.42
P–O'	1.72	1.94
P–O''	1.62	1.74
O–O''	1.57	1.65
H''–P–O'	97.6	94.7
O'–P–O''	56.1	53.1
O''–P–H'	97.3	99.1

The effects of sterically bulky R substituents are more difficult to anticipate, but it can be expected that increased steric congestion will tend to planarize the PR_3 pyramid. In accordance with Bent's rule, this geometrical change should redirect s-character to the P–R bonds and p-character to the P–O bonds, thus tending to oppose the P–R polarity effects described above, reducing the linearity of the O–P–R linkages and weakening the $n_{O'} \rightarrow \sigma^*_{PR'}$ and $n_{O''} \rightarrow \sigma^*_{PR''}$ interactions. Beyond these rather local and generic substituent influences on phosphorus bonding, more difficult questions can be raised concerning possible “remote” substituent contacts with the PO_2 moiety, particularly those associated with OCH_3 and CF_3 groups in the ortho position of bulky aryl substituents (cf. Selke et al.⁴). Such possible effects of remote substituent contact with the PO_2 moiety are beyond the scope of the present treatment.

Optimizations and Population Analysis without d-Functions. As an alternative measure of d-orbital participation in O_2PH_3 , a second geometry optimization was performed without polarization functions using the 6-31+G basis set. The species was confirmed to be a true equilibrium structure by verifying that all vibrational frequencies are positive and also by checking the wave function for electronic instability using the STABLE=OPT keyword. Although the d-free bond lengths increase somewhat (Table 4), the species retains essentially the same C_s -symmetric, pentacoordinated structure, demonstrating that d-functions are not necessary for determining the qualitative

(42) Bent, H. A. *Chem. Rev.* **1961**, *61*, 275–311; see ref 25, pp 138–146.

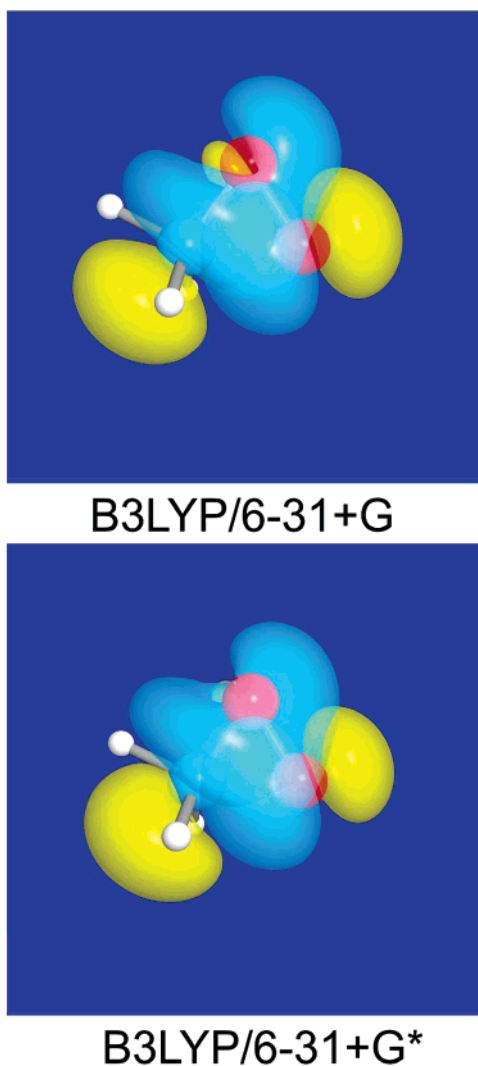


Figure 9. Three-dimensional surface view of outer contour for the $n(\text{O}') \rightarrow \sigma^*(\text{P}-\text{O}'')$ interaction without d-orbitals (left) and with d-orbitals (right).

Table 5. NRT Bond Orders for O_2PH_3 in 7-Reference Treatment

A-B	b_{AB} Bond Order	
	6-31+G*	6-31+G
P-H'	0.79	0.82
P-H''	0.88	0.90
P-O'	0.52	0.34
P-O''	0.72	0.75
O'-O''	1.05	1.08

aspects of the electronic structure. Furthermore, the same three-center bonding motifs appeared, with relatively minor differences ($\sim 25\%$) in the strength of the delocalizations. A comparison of the overlap plots with and without polarization functions for the $n_{\text{O}'} \rightarrow \sigma^*_{\text{PO}'}$ interaction (Figure 9) demonstrates that the qualitative aspects of the inner-lobe three-center bonding remain essentially preserved. The general consistency of the electronic structure with and without polarization functions is also reflected in the NRT bond orders from the 7-Ref calculation (Table 5) and non-Lewis electron occupancies of the reference structures (Table 6).

Some discrepancies, however, do occur between the 6-31+G and 6-31+G* calculations, most notably in the decrease of P-O' bond order from 0.52 to 0.34 (Table 5). At 6-31+G*, the

Table 6. NRT Total Non-Lewis Occupancies (ρ_{NL}) for Reference Structures I–V

structure	ρ_{NL} (e)	
	6-31+G*	6-31+G
I	0.64	0.85
II	0.60	0.53
III	0.77	0.87
IVa	1.14	1.19
IVb	1.37	1.41
IVc	1.37	1.41
V	3.99	2.17

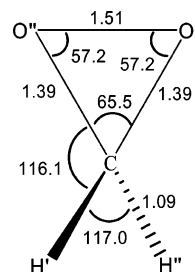


Figure 10. Bond lengths (Å) and bond angles (deg) for O_2CH_2 at the B3LYP/6-31+G* level.

$n_{\text{O}'} \rightarrow ry^*_{\text{P}}$ delocalization has a Fock matrix value of $F_{ij} = 0.18$ au and perturbative energy strength of 27.2 kcal/mol. The most likely contributor to the loss of P-O' bond order is therefore the complete removal of this interaction. Furthermore, in structure **II**, the P-H' and P-O' bonds both have approximately 3% d-character at 6-31+G*. The loss of freedom to deform the pure sp hybrids with polarization functions is exemplified by the slightly altered form of the inner lobe of the P-O' antibond (Figure 9). The $n_{\text{O}'} \rightarrow \sigma^*_{\text{PH}'}$ and $n_{\text{O}'} \rightarrow \sigma^*_{\text{PO}'}$ interactions are weakened as a result, causing the Fock matrix elements to decrease from 0.16 to 0.12 au for both delocalizations. Therefore, while d-orbitals do not contribute at the level of full hybridization, they participate as significant polarization functions to better describe off-axis deformation of the strained valence NBOs, thereby contributing noticeably to the electronic structure and molecular geometry.

Dioxirane (O_2CH_2) Analogue. It is instructive to compare the resonance description and molecular geometry of phosphadioxirane, an onium peroxide, to the parent dioxirane (O_2CH_2), an enium peroxide. At B3LYP/6-31+G*, dioxirane is calculated to be C_{2v} -symmetric, with equivalent oxygens and hydrogens (Figure 10). The geometry is consistent with a slight distortion from idealized tetrahedral sp^3 hybrids at carbon.

In the parent dioxirane O_2CH_2 , **I** is by far the dominant resonance structure, accounting for over 91% of the electron density (Table 7). Furthermore, the ion pair and zwitterionic structures have negligible weightings. Structure **I** therefore dominates the resonance description. The cyclic geometry is well described by a single, valence shell description with p-rich hybrids directed toward the oxygens and s-rich hybrids directed toward the hydrogens (Table 8). This results in full double occupancy and bond orders near unity for both the C-C and C-O NBOs.

The resonance description of dioxirane therefore offers an obvious contrast to phosphadioxirane. In dioxirane, an enium peroxide, cyclization can be accomplished within the valence shell, and cyclic structure **I** provides a nearly complete localized

Table 7. NRT Resonance Weightings for Peroxidic Structures of Dioxirane

	I	II	III	IVa	IVb	V
Dioxirane^a	91.6	<1.0	<1.0	<1.0	<1.0	<1.0

^a Reference: all dioxirane structures I–IV.

Table 8. Carbon-Based σ -Bond NBOs and Occupancies (total and d -type) for Structure I, Showing Polarization Coefficient (c_c) and Hybrid (h_c) (with percent $s/p/d$ Character) for Each $\sigma_{CX} = c_c h_c + c_X h_X$

NBO	Occupancy		bond order	c_c	h_c	% s	% p	% d
	total (e)	d_c (e)						
C–H	2.00	0.00	0.98	0.78	$sp^{2.1}d^{0.0}$	32	68	0
C–O	1.99	0.00	1.00	0.58	$sp^{4.6}d^{0.0}$	18	82	0

description of the electron density. The most important delocalizations within the dioxxygen ring of O_2CH_2 are therefore geminal $\sigma \rightarrow \sigma^*$ delocalizations between the C–O and O–O bonds.⁴³ Meanwhile, in phosphadioxirane, an onium peroxide, cyclization violates the octet rule, and the valence-shell-conforming structures II–IVc become much more important than I in the resonance description. To avoid the use of energetically costly d -orbitals, phosphadioxirane is a delocalized composite of several *ionic* resonance structures. The strongest stabilizing interactions in the phosphadioxirane ring are therefore $n \rightarrow \sigma^*$ delocalizations from the oxygen lone pairs into the P–O antibonds. Analogous questions could be raised for other R_nXO_2 species (e.g., X = sulfur; see Supporting Information), but such analogues are beyond the scope of the present work.

Summary and Conclusions: Structure and Nomenclature of Phosphadioxiranes

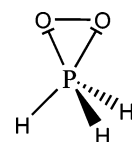
Nominal phosphadioxiranes present fascinating challenges both in understanding their chemical behavior and in formulating accurate localized structural representations of their electronic structure. In the present work, we have employed an array of NBO/NRT-based analysis tools in conjunction with *ab initio* and hybrid density functional calculations to investigate the puzzling structural and reactivity issues presented by these species. Specifically, we have considered a range of possible resonance structure representations of phosphadioxiranes as well as kindred enium and onium peroxides in order to quantify aspects of their apparent hypervalency (specifically, the role of extra-valence d -orbitals in skeletal hybridization) and to identify specific NBO donor–acceptor interactions that could account for their primary resonance delocalizations and structural tendencies.

In accordance with previous studies of apparent main-group hypervalency, we find that true hypervalent character (i.e., significant d -orbital participation in skeletal hybridization) is rather negligible in phosphadioxiranes. Indeed, the calculated geometry and resonance weightings in O_2PH_3 and its derivatives are found to remain essentially unchanged upon removal of all d -functions from the variational calculation. Instead, the apparent hypervalency is found to be accomplished by two distinct types of $3c/4e$ ω -bonds: the first ($^-H: ^+P-O \leftrightarrow H-P^+ :O^-$) is of unsurprising linear type, but the second ($^-O: ^+P-O \leftrightarrow O-P^+ :O^-$) is of unprecedented *cyclic* type. [A third,

weaker nonlinear hyperbond is also observed ($^-H: ^+P-O \leftrightarrow H-P^+ :O^-$) in a resonance between structures III and IVa.] NBO orbital plots clearly show that this resonance-type delocalization is accomplished through $n \rightarrow \sigma^*$ delocalizations from the oxygen lone pair to the *middle* lobe of the antibond, in contrast to typical $n \rightarrow \sigma^*$ interactions involving the more favorably exposed backside lobe. The observed three-center interactions are fully consistent with the observed lack of acyclic equilibrium geometries. Additional linear hyperbonds of ω_{OPH} -type involving the substituents offer incremental stability that is absent in open structures, while the cyclic ω_{OPO} bonds alleviate the ring strain and strongly promote cyclization.

The diffuseness of the lone pairs and the exposure of the antibond are expected to vary with the electronegativity of the phosphine substituents. In substituted phosphadioxiranes (see Supporting Information), the important $n \rightarrow \sigma^*$ interactions are therefore weakened or strengthened with a corresponding change in the weighting of the resonance structures involved. Despite minor variations, the qualitative picture of linear and cyclic $3c/4e$ hyperbonding remains the same across various substituents.

The most common Lewis structure representation I and associated phosphadioxirane nomenclature is therefore somewhat inaccurate as a description of the O_2PH_3 electronic structure, suggesting a degree of hypervalency and valence shell expansion that is not supported by the calculations. How could the cyclic $3c/4e$ bonding pattern best be represented in a single structural diagram? We propose the following modified Lewis structure for phosphadioxirane involving a *bent* ω -bond (I-bond)⁴⁴ notation for $3c/4e$ interactions.²⁵



In light of the computational results, it appears that O_2PH_3 is more accurately represented as a “hyperperoxo complex of phosphine” to suggest the essential O–O single bond character of the complexing group and distinctive *hyperbonding* ($3c/4e$ resonance) coordinative attachment to the parent phosphine species, corresponding to the structural ω -bonded depiction given above. The revised Lewis structure and “hyperperoxo-phosphine” nomenclature seem better able than former “phosphadioxirane” depictions to suggest the key electronic features

(43) A geminal $\sigma \rightarrow \sigma^*$ interaction (e.g., of $\sigma_{AX} \rightarrow \sigma^*_{AY}$ form) arises between the apically joined bond (σ_{AX}) and antibond (σ^*_{AY}) orbitals that share a common center (e.g., in X–A–Y bond connectivity), corresponding to $^2J_{XY}$ -type scalar NMR coupling. Such interactions may be distinguished from the more common vicinal ($^3J_{XY}$) $\sigma_{AX} \rightarrow \sigma^*_{BY}$ interactions of X–A–B–Y bond connectivity. For a more thorough discussion of geminal delocalizations, see ref 25, pp 263–275.

(44) Epiotis, N. D. *Deciphering the Chemical Code*; VCH Publishers: New York, 1996.

that distinguish O_2PH_3 from nonhypervalent peroxides as well as weakly coordinated peroxy complexes of main-group elements. Even the improved diagram, however, fails to completely represent the unique combination of linear and cyclic ω -bonding that contributes to the observed coordination geometry and chemical reactivity of these remarkable species.

Acknowledgment. We thank Clark Landis, Shannon Stahl, Christine Morales, and Joe Wildenberg for useful discussion.

Supporting Information Available: Complete ref 39. Geometries, energies, and resonance descriptions for several phosphadioxirane derivatives ($R = F, CN, CH_3, C_2H_5$) are included in the Supporting Information. A discussion of sulfur analogues (thiadioxirane) is also included. This material is available free of charge via the Internet at <http://pubs.acs.org>.

JA060676F